-RESEARCH PAPER-

International Journal of Mining and Geo-Engineering

IJMGE

IJMGE 60-3 (2026) 259-265

DOI: 10.22059/ijmge.2026.404658.595327

Efficient computation of the ERT sensitivity matrix via a semi-analytical approach

Yosra Azadi [a], Reza Ghanati [a,*], and Mahdi Fallahsafari [a]

[a] *Institute of Geophysics, University of Tehran, Tehran, Iran.*

Article History:

Received: 20 October 2025.

Revised: 24 December 2026.

Accepted: 13 May 2026.

ABSTRACT

The partial derivative of data with respect to model parameters also known as the Jacobian or sensitivity matrix plays a significant role in electrical resistivity tomography inversion by which the influence of a differential model parameter change on individual measurements is denoted. Hence, providing the sensitivity matrix is a crucial step in the 2D/3D electrical resistivity tomography inversion process. While the sensitivity matrix is extensive, calculating each individual sensitivity associated with every cell (or model parameter) is computationally expensive which may not feasible in the case of large model space. There is always a challenge in keeping the accuracy of the analytical method while reaching a reasonable computing time. This paper proposed a semi-analytical method to reduce the sensitivity matrix calculation time compared to the conventional method. The integration over the signal contribution which is the most time-consuming part of the sensitivity calculation, was solved using the Modified Gauss–Legendre quadrature (MGLQ) method. To verify the functionality of the proposed approach, the sensitivity distribution of an isotropic and homogeneous model was displayed for three common electrode configurations, i.e., pole-pole, dipole-dipole, and Wenner arrays. Our investigation demonstrate that the sensitivity values vary spatially depending on the type of electrode positions. Furthermore, when employing a semi-analytic scheme, the proposed algorithm delivers a substantial reduction in computation time while maintaining acceptable accuracy in the calculated values. The presented method can be readily extended to other electrode configurations with arbitrary subsurface conductivity distribution.

Keywords: *ERT, Gaussian quadrature, Modified gauss–legendre quadrature, Sensitivity matrix*

1. Introduction

The calculation of the sensitivity matrix in electrical resistivity tomography (ERT), also referred to as the Jacobian Matrix, is a critical component in the inversion process, model appraisal of the reconstructed model, and the interpretation of measurement data. The sensitivity matrix must be computed for every nonlinear inversion to assess how changes in resistivity affect the potential measurements. Additionally, sensitivity values are instrumental in evaluating the accuracy and quality of the inverted resistivity tomograms. The sensitivity matrix is derived from the ratio of the change in potential to the change in resistivity for each cell within a mesh grid. These partial derivatives constitute the individual elements of the matrix. Even small errors in the matrix values can lead to substantial inaccuracies in the final inversion model. Furthermore, the extensive calculations required, coupled with the computational complexity, can result in significant processing times. As such, selecting an appropriate computational method is paramount for ensuring a successful and computationally feasible inversion of the measured data. To address this challenge, the integration of potential contributions (the most computationally demanding aspect of sensitivity calculation) is often performed using a numerical scheme known as the Gaussian Quadrature method. This revision clarifies some scientific points while maintaining the integrity of the original ideas.

The early solution of the Fréchet derivative integral (or sensitivity distribution) dates back to [1]. In practice, these integrals must be evaluated numerically using Gaussian Quadrature for multiple integrals. This method is generally regarded as an efficient and accurate approach for evaluating most functions. There are three primary numerical methods for sensitivity calculation: 1) the perturbation method, 2) forward sensitivity calculation, and 3) the adjoint equation method. Additionally, one analytical method exists. The numerical methods are applicable to arbitrary resistivity distributions while the analytical approach is typically restricted to homogeneous resistivity distributions [2]. Among these methods, we calculate the sensitivity matrix using a semi-analytic technique which combines the accuracy of the analytical solution with the efficiency of a numerical approach. With the development of 2D and 3D resistivity investigations, various authors have discussed the sensitivity calculation in ERT, often in conjunction with inversion techniques, though rarely as a standalone topic. The first work on sensitivity functions was presented by [3], who computed sensitivity values for a homogeneous subsurface. [4] calculated the Fréchet derivatives within the framework of single scattering theory. It was conducted [5] a comparative study on the application of different techniques for sensitivity calculations in 1D and 2D resistivity problems, and was extended [6] this analysis to 3D cases. [7] proposed a 3D resistivity inversion using the finite-element method, incorporating a coarse 3D sensitivity plot for a dipole-dipole array. [8] demonstrated that sensitivity values could be computed using finite-difference forward modeling to account for any arbitrary conductivity distribution. [2] examined several methods for calculating sensitivities in both homogeneous and inhomogeneous cases, highlighting significant deformations in sensitivity distributions due to high conductivity contrasts. [9] and [10] addressed the calculation of the sensitivity function using DC forward modeling. [11], [12], and more recently, [13] discussed the key properties of sensitivity sections for cross-hole

* Corresponding author. *E-mail address:* rghanati@ut.ac.ir (R. Ghanati).

electrode arrangements. Most recently, [14] proposed a numerical method based on the forward matrix approach for calculating Fréchet derivatives in the context of ERT.

Despite successful efforts to solve the sensitivity function, the calculation of Fréchet derivatives in ERT remains an active and promising area of research. The primary aim of this study is to provide an accurate scheme for calculating sensitivity values while also exploring the sensitivity properties of traditional geo-electrical arrangements from both computational and theoretical perspectives. To this end, a semi-analytic approach known as the Modified Gauss–Legendre quadrature (MGLQ) method is proposed, which leverages the reciprocity principle of electrical resistivity tomography within the framework of a finite difference method. The sensitivity values for a 2D homogeneous subsurface are computed for various electrical configurations. Furthermore, to reduce computational time during the calculation of each sensitivity matrix element, several optimization techniques are introduced, which will be discussed in detail in later sections.

The paper is structured as follows: Section 2 provides a comprehensive description of the numerical procedure used to calculate the sensitivity matrix. Section 3 presents the numerical results for a homogeneous half-space model, using commonly employed field arrays (e.g. Pole-Pole, Dipole-Dipole, and Wenner configurations), along with an analysis of the corresponding sensitivity patterns. Section 4 presents the results, emphasizing the computational efficiency improvements achieved with the MGLQ method, its validation against traditional approaches, and the analysis of sensitivity patterns across various electrode arrays. Section 5 then provides a concise conclusion.

2. Materials and Methods

In this study, we used the MGLQ method, which incorporates analytical techniques for singularity management (Appendix A) and reduces computational time by eliminating the need for the time-consuming adaptive method to calculate the sensitivity matrix for three different electrode configurations. This method reducing computational costs during sensitivity matrix assembly uses predefined nodes and weights for accurate two-dimensional integration and handles singularities near the electrodes with specific analytical techniques. Our approach is benchmarked against MATLAB's standard adaptive Gauss-Kronrod quadrature (AGKQ). While the AGKQ technique efficiently control integration error for well-behaved integrands, they do not explicitly account for or manage singularities within the integration domain. The advantage of singularity management is that it improves speed by reducing the need for additional calculations in sensitive areas, such as near electrodes. Moreover, MGLQ is expected to be faster than the conventional method when using a specific number of nodes (n_GL) in both dimensions, as it avoids recalculating integration points and grid adjustments. Through the comparison, we found that using 4 nodes provides a good balance between speed and accuracy, making it an efficient choice for our problem [15]. Furthermore, precomputing the nodes and weights improves numerical integration efficiency by avoiding repeated calculations and reducing computational cost.

2.1. Two-dimensional Gaussian Quadrature method

The 2D Gauss-Legendre Quadrature method is a powerful numerical approach for evaluating definite integrals, particularly useful for two-dimensional integrals encountered in ERT. This method approximates the integral by summing the values of the integrand at specific points, known as nodes (or abscissas), within the integration domain. These nodes are strategically selected to optimize the accuracy of the approximation, with corresponding weights determining the contribution of each node in the sum. For two-dimensional integrals, the Gauss-Legendre Quadrature is extended by applying the rule in both directions, typically along the x and z axes. The double integral is then approximated as follows:

$$U = \int_{x_1}^{x_2}\int_{z_1}^{z_2} f(x,z)dzdx \approx \sum_{i=1}^{n}\sum_{j=1}^{n} w_x(i)w_z(j)f(x_i,z_j), \qquad (1)$$

where w_x and w_z are the weights associated with the x and z directions, respectively, and x_i, z_j are the nodes in those directions. The nodes and weights are generally derived from solving the Legendre differential equation, and for a specific number of nodes, these values can be precomputed to streamline the process. In practical applications, such as in ERT, the nodes, initially defined on the standard interval [-1,1], are mapped to the physical domain through an affine transformation to account for real-world integration bounds.

By utilizing this quadrature method, the integration process in complex models, such as those found in ERT, can be efficiently carried out while maintaining a high level of accuracy, especially when evaluating integrals over large grids of model parameters [16].

2.2. Calculation of the sensitivity matrix

The electrical resistivity tomography inverse problem is a non-linear process and no matter what method we use for our inversion problem, calculating the sensitivity values is inevitable. According to [17] a single sensitivity value (Γ_{ij}) represents the change of forward response φ_i as a function of the model $\mathbf{m}$ with respect to a change of the model parameter $\mathbf{m}_j$.

$$\Gamma_{ij}(\mathbf{m}) = \frac{\partial\varphi_i(\mathbf{m})}{\partial \mathbf{m}_j} \qquad (2)$$

Thus, the sensitivity matrix is given as:

$$\Gamma = \begin{pmatrix} \frac{\partial\varphi_1(\mathbf{m})}{\partial \mathrm{m}_1} & \cdots & \frac{\partial\varphi_1(\mathbf{m})}{\partial \mathrm{m}_m} \\ \vdots & \ddots & \vdots \\ \frac{\partial\varphi_n(\mathbf{m})}{\partial \mathrm{m}_1} & \cdots & \frac{\partial\varphi_n(\mathbf{m})}{\partial \mathrm{m}_m} \end{pmatrix}_{m\times n} \qquad (3)$$

where the dimensions of the sensitivity matrix correspond directly to the number of potential measurements (rows) and model parameters (columns). During each iteration of the inversion process, this matrix serves as the foundation for updating the model parameters. There are a few numerical approaches to calculate the sensitivity function. The computation of the sensitivity matrix is strongly related to the method of forward modeling. In this paper, we utilize the reciprocity principle of electrical impedance tomography, introduced by [18], to demonstrate how the apparent resistivity ρ_a changes due to a change of the resistivity ρ. The sensitivity function in the anomalous Ω_i is defined as [6].

$$\Gamma = \frac{\delta\rho_a}{\delta\rho} = \frac{G}{\rho^2}\iiint_{\Omega_i} \frac{\vec{\nabla}\varphi}{I_\varphi}\cdot\frac{\vec{\nabla}\psi}{I_\psi}\,\vec{d}^3r, \qquad (4)$$

where ρ_a is the forward response (apparent resistivity), ρ is the resistivity derived from the inversion process, G is the geometry factor, φ is the electrical potential caused by injecting the current I_φ, ψ is the electrical potential caused by interchanging source and receiver electrodes through the current I_ψ, and r is the cell position (x, y, z) with respect to the source position.

Assuming a two-dimensional homogeneous model where the model cells have infinite extent in the y-direction, the unbounded integration along the y-axis can be converted to a bounded form through the use of complete elliptic integrals of the first $K(k)$ and second $E(k)$ kinds. [17] demonstrated that for a pole-pole array configuration, the sensitivity function can be expressed in terms of these elliptic integrals which written as:

$$\mathrm{S}(x,z) = \frac{1}{4\pi^2}(M_1[(x-x_A)(x-x_M)+z^2]+M_2) \qquad (5)$$

where M_1 and M_2 are defined as:

$$M_1 = \frac{2}{ab^2(a^2-b^2)^2}[(a^2+b^2)E(k) - 2b^2K(k)] \qquad (6)$$

$$M_2 = \frac{2}{a(a^2-b^2)^2}[(a^2+b^2)K(k) - 2a^2E(k) \qquad (7)$$

In Equations (5-7), x_A and x_M are the position of the current and potential electrodes, respectively. In addition, the parameters a, b, and

k are defined as:

$$a^2 = \max\{(x - x_A)^2 + z^2, (x - x_M)^2 + z^2\} \quad (8)$$

$$b^2 = \min\{(x - x_A)^2 + z^2, (x - x_M)^2 + z^2\} \quad (9)$$

$$k = 1 - \frac{b^2}{a^2} \quad (10)$$

Note that $K(k)$ and $E(k)$ are elliptical complete integrals of the first and second order, respectively [19]. Calculating the Jacobian matrix for an array with more than two electrodes is quickly carried out by using the pole-pole results with the appropriate spacing (Appendix B). Assuming the $x - y$ plane coincides with the ground surface, we get:

$$J_{ij} = \int_{z_i}^{z_{i+1}} \int_{x_j}^{x_{j+1}} \Gamma_{ij}.dx.dz \quad (11)$$

where J_{ij} is the Jacobean matrix. The numerical integration process across all model elements constitutes the most computationally intensive aspect of our forward modeling problem. While conventional numerical methods can adequately solve these integrals, their computational demands become prohibitive for large model spaces, necessitating the development of an optimized approach. We selected the Gaussian Quadrature method for its exceptional combination of precision and computational efficiency which is particularly well-suited for our application. The method's effectiveness stems from its use of precomputed weights and abscissas [20], determined through solution of the Legendre differential equation. The eigenvalues and eigenvectors obtained from this solution directly provide the integration parameters for a specified number of quadrature points (n_{GL}).

2.3. Semi-analytical approach

In the MGLQ method, a semi-analytical approach is used to compute the sensitivity matrix in ERT. The term "semi-analytical" refers to the hybrid strategy that combines analytical solutions for handling singularities near electrodes with numerical methods applied in other regions of the model. Pre-defined nodes and weights are utilized for precise two-dimensional integration, particularly in regions adjacent to the electrodes where sensitivity calculations are critical due to sharp variations in the electric field. Analytical methods are specifically employed to address these singularities. The key advantage of this approach is its enhanced computational efficiency, which is achieved without sacrificing the accuracy of sensitivity calculations. Further details on this process and the methods used to handle singularities are provided in Appendix A. This approach significantly reduces processing time, particularly in large-scale models with numerous sensitivity elements where computational speed is a crucial factor.

2.4. Discretization and Algorithm

The model used in this study follows a rectangular grid arrangement, as described by [21]. The computational domain is discretized using a grid defined by the x- and z-coordinates, with step sizes of $\Delta x = 0.1$ and $\Delta z = 0.01$. This grid resolution ensures sufficient detail to accurately represent the model for numerical analysis. The MGLQ method is employed for integration, utilizing an equal number of nodes (n_{GL}) in both the x- and z-directions to maintain consistency across the two dimensions. This approach calculates the system's sensitivity over the discretized grid while incorporating singularity handling techniques for regions near the electrodes, thereby optimizing both efficiency and accuracy. All numerical algorithms were implemented in MATLAB R2022a and executed on a desktop computer with an Intel® Core™ i5-8400 CPU (6 cores, 2.80 GHz) and 16 GB of RAM.

2.5. Accuracy Verification

This study employs the reciprocity theorem to validate the model and ensure computational accuracy. The theorem asserts that the sensitivity of a measurement between electrodes M and N, resulting from a current injected between electrodes A and B, should be equivalent to the sensitivity of the measurement between A and B when the current is injected between M and N. This relationship is mathematically expressed as:

$$J^n(A, B, M, N) \approx J^r(M, N, A, B) \quad (12)$$

where J^n and J^r represent the sensitivity values corresponding to the normal and reverse measurements, respectively. To validate the implementation, the relative L_2-norm of the difference between the two computed sensitivity values, defined as:

$$\delta = \frac{\|J^n - J^r\|_2}{\|J^n\|_2}. \quad (13)$$

is calculated and compared against a stringent tolerance criterion.

3. Numerical Examples

This section presents a comprehensive comparison between the proposed MGLQ method and the conventional AGKQ method, focusing on three primary objectives: first, to validate the accuracy of the MGLQ algorithm; second, to assess its computational efficiency; and third, to provide a geophysical interpretation of the sensitivity patterns for different electrode arrays. The numerical accuracy of our implementation was initially verified through the reciprocity theorem which resulted in an error of approximately 0.2%. This confirms that the method adheres to fundamental physical principles, establishing the reliability of the algorithm for subsequent analysis.

Next, we demonstrate the superior computational efficiency of our algorithm by testing it with three widely recognized electrode arrays. The sensitivity values of a homogeneous resistivity model, characterized by a constant resistivity of $\rho = 20\,\Omega.\mathrm{m}$, for various electrical configurations such as Pole-Pole, Dipole-Dipole, and Wenner arrangements are calculated (Table 1). The sensitivity analysis is performed to examine how each configuration responds to changes in subsurface resistivity. For all electrode configurations, we use an identical gridding system with consistent step sizes in both x and z-directions, ensuring a fair comparison. The forward calculations which simulate the relationship between applied currents and measured potentials, are carried out using the same numerical approach for each configuration, allowing us to compare their sensitivity patterns directly. As shown in Table 1, the MGLQ method significantly reduces processing time compared to the AGKQ approach across different electrode arrays such as Pole-Pole, Dipole-Dipole, and Wenner. We observed a 15- to 16-fold reduction in computation time per integration when using the MGLQ method, as compared to the AGKQ approach. Through systematic testing, we established $n_{GL} = 4$ nodes as providing an optimal balance between speed and accuracy, making it an efficient choice for our problem. While higher values of nodes could improve precision, the marginal improvement did not justify the additional computational cost.

The results indicate that the computation time for a single data point is considerably reduced with the optimized method. When applied to real-world scenarios with large datasets, this improvement would result in a dramatic decrease in computational costs, making the process more efficient and cost-effective. In other words, these results highlight the significant enhancements in computational efficiency which could be a critical factor in geophysical inversion problems, where computational resources are often a limiting factor in model resolution and scalability. Having established the computational efficiency of the MGLQ method, we now turn to our second objective: the analysis and interpretation of sensitivity patterns. The following three examples illustrate the application of our method to classic electrode arrays, pole-pole, dipole-dipole, and Wenner, in a homogeneous half-space. These examples serve to validate the numerical accuracy of the MGLQ algorithm by comparing the computed sensitivity distributions against well-established theoretical expectations for each configuration.

3.1. Example 1

The first example examines the sensitivity pattern for a pole-pole array in a homogeneous half-space model ($\rho = 20\,\Omega.m$). The current

electrode is positioned at $x = 2\,m$ and the potential electrode at $x = 8\,m$, with $d = 5$ m-electrode spacing used for the sensitivity calculations. Figure 1(a) presents the resulting sensitivity distribution computed using the MGLQ algorithm, showing negative sensitivity values between the two electrodes (source and receiver) and positive values elsewhere, as theoretically expected. Figure 1(b) shows the resulting sensitivity distribution computed using the AGKQ algorithm. In addition, Figure 1(c) presents the result of difference in sensitivity distribution between two methods that clearly demonstrates the agreement between the results, highlighting a trivial difference in this case. From the observations, the strongest sensitivity variations occur directly beneath the electrodes, with values diminishing progressively at greater distances. The sensitivity patterns reveal that the pole-pole configuration provides extensive horizontal coverage and significant depth of investigation. However, this comes at the cost of reduced vertical and horizontal resolution, evident from the wide spacing between sensitivity contours. These sensitivity distributions serve as valuable tools for evaluating inversion reliability, offering a practical alternative to computationally intensive full resolution matrices. By analyzing the sensitivity matrix, comprising a data weighting matrix and the Jacobian matrix for the final model, we can identify well-constrained regions (high sensitivity values) versus poorly constrained areas (low sensitivity values) in the inverted model [22]. This approach enables more confident interpretation of inversion results, with high-sensitivity regions warranting greater trust in the derived model parameters. Additionally, the calculated reciprocity error is $\delta = 0.17\%$, demonstrating the minimal deviation between the sensitivity results when the electrode configuration is reversed, as expected by the Reciprocity Theorem.

3.2. Example 2

The second example analyzes the sensitivity function for a Dipole-Dipole array over a homogeneous half-space (ρ = 20 Ω.m), with parameters set to d = 2 m and n = 1. The sensitivity distribution computed using the proposed MGLQ algorithm is shown in Figure 2(a). The pattern exhibits the expected theoretical behavior, with negative sensitivity values between the current and potential electrode pairs and positive values between pairs of the same type. For comparison, Figure 2(b) presents the corresponding result from the conventional AGKQ algorithm. The difference between the two results, shown in Figure 2(c), is minimal, confirming a strong numerical agreement and validating the accuracy of the MGLQ method. The resulting pattern shows that sensitivity varies significantly across the domain. High-sensitivity zones correspond to well-constrained regions in an inversion, yielding more reliable results while low-sensitivity areas (approaching zero) indicate poorly constrained regions. The distinct vertical orientation of the sensitivity contours makes this configuration particularly effective for resolving vertical structures such as dikes and geological contacts. However, this characteristic also results in a shallower overall depth of investigation compared to the pole-pole array. In addition, the calculated reciprocity error is δ=0.19%, reflecting a small deviation between the sensitivity results.

3.3. Example 3

The third experiment investigates the sensitivity patterns of the Wenner array over a homogeneous half-space with a resistivity of 20 Ω.m. The configuration uses an electrode spacing of d = 2 m and a separation factor of n = 1. Figure 3(a) displays the sensitivity distribution computed using the MGLQ algorithm, revealing a pattern with a dominant horizontal orientation. For comparison, the result from the conventional AGKQ method is shown in Figure 3(b). The difference between the two, presented in Figure 3(c), is minimal, confirming the consistency and numerical accuracy of the MGLQ implementation. The sensitivity distribution shows positive values between the potential electrode pairs and negative values between the current and potential electrodes. The highest sensitivity is concentrated directly beneath the electrodes and diminishes radially with distance. This horizontal sensitivity pattern makes the Wenner array highly effective for characterizing horizontal layers but provides poor resolution for vertical structures such as dikes or contacts. Compared to the dipole-dipole array, the Wenner configuration yields higher overall sensitivity, enhancing measurement reliability. Its depth of investigation is greater than the dipole-dipole array's but shallower than the pole-pole array's. Furthermore, the Wenner array produces denser and more focused sensitivity contours than the pole-pole configuration, resulting in superior lateral resolution. These characteristics establish the Wenner array as an excellent choice for vertically layered subsurface investigations. Furthermore, the calculated reciprocity error is δ=0.19%, showing a negligible difference between the sensitivity results.

Table 1. Integration runtime (in second) for f(x,z) over x = [0,10] and z = [0, 2] in a homogeneous 20 Ω · m half-space, comparing a 4×4 MGLQ scheme ($n_{GL} = 4$) with the AGKQ method on identical grids across Pole–Pole, Dipole–Dipole, and Wenner arrays. The Parameters n and d are separation level and electrode spacing, respectively.

Array Type	Parameters (n, d)	MGLQ	AGKQ	Speedup
Pole-Pole	d = 5	0.741	11.399	15
Dipole-Dipole	n = 1, d = 2	1.464	22.909	16
Wenner	n = 1, d = 2	1.461	22.992dd	16

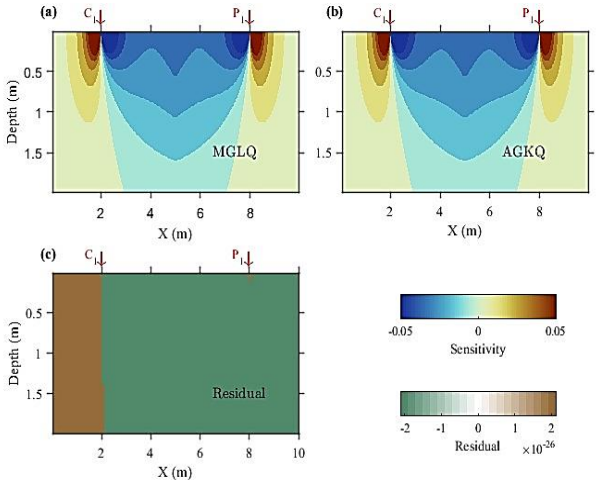

Figure 1. Sensitivity pattern for a pole-pole array in a homogeneous half-space (ρ = 20 Ω. m). Results are shown for (a) the MGLQ method, (b) the AGKQ method, and (c) the difference between them. The red arrows indicate the positions of the current and potential electrodes.

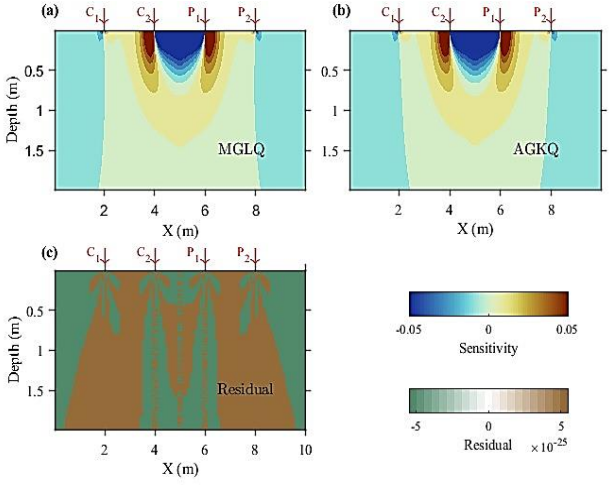

Figure 2. Sensitivity pattern for the Dipole-Dipole array in a homogeneous half-space ($\rho = 20\ \Omega.m$). Results are shown for (a) the MGLQ method, (b) the AGKQ method, and (c) the difference between them. The red arrows indicate the positions of the current and potential electrodes.

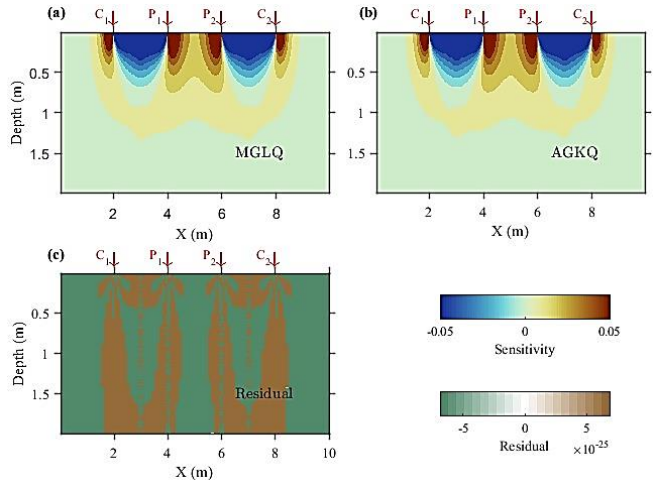

Figure 3. Sensitivity pattern for the Wenner array in a homogeneous half-space ($\rho = 20\ \Omega.m$). Results are shown for (a) the MGLQ method, (b) the AGKQ method, and (c) the difference between them. The red arrows indicate the positions of the current and potential electrodes.

4. Discussion

This study has demonstrated that the MGLQ method offers a computationally superior alternative to the AGKQ algorithm for calculating the sensitivity matrix in ERT. The discussion below interprets these results in the context of the study's dual objectives: computational efficiency and sensitivity pattern analysis. The primary achievement of the MGLQ method is its dramatic reduction in computation time, achieving a 15- to 16-fold speedup across all tested electrode arrays (Table 1). This efficiency stems from several key design choices. First, the use of a fixed number of Gauss-Legendre nodes (n_GL = 4) in a 4×4 scheme eliminates the dynamic grid adjustments and recursive calculations inherent in adaptive methods like AGKQ. Second, the precomputation of nodes and weights streamlines the integration process. Most importantly, the explicit analytical handling of singularities at electrode positions prevents the AGKQ method's performance degradation in these critical regions where it would otherwise be forced to expend significant computational effort to achieve convergence. This integrated approach, combining a fixed, efficient quadrature rule with targeted analytical solutions, provides a robust framework for rapid sensitivity calculation which is directly scalable to large-scale 2D and 3D inversion problems where the sensitivity matrix must be computed repeatedly. The computational speed of the MGLQ method would be irrelevant without a concurrent guarantee of accuracy. Our results provide multiple layers of validation. The strong agreement between the MGLQ and AGKQ sensitivity distributions, evidenced by the minimal differences in Figures 1(c), 2(c), and 3(c), confirms that the MGLQ method does not sacrifice precision for speed. Furthermore, the reciprocity validation which shows lower than 0.2% error, demonstrates that the method adheres to fundamental physical principles to within remarkable precision. This successful validation against both a conventional numerical method and a core physical theorem underscores the numerical robustness of the proposed semi-analytical approach.

The third objective of this study was to interpret the sensitivity patterns of common electrode configurations, thereby showcasing the practical utility of the computed matrix. The results for the pole-pole, dipole-dipole, and Wenner arrays align perfectly with established geophysical theory, which further validates the correctness of our algorithm. The analysis confirms that the pole-pole array provides the greatest depth of investigation but with diffuse resolution, making it suitable for regional reconnaissance. In contrast, the dipole-dipole array produces vertically oriented sensitivity contours, ideal for imaging steeply dipping structures like dikes, albeit with a shallower investigation depth. The Wenner array, with its horizontally focused sensitivity and superior lateral resolution, proves optimal for characterizing layered structures. These observations are not merely theoretical; they provide crucial guidance for survey design by linking specific array geometries to their resolving capabilities for different geological targets. The sensitivity matrix, therefore, serves as a powerful tool for pre-survey planning and for qualitatively assessing the reliability of inversion results by identifying well-constrained and poorly-constrained regions of the subsurface model.

5. Conclusion

This study has successfully developed and validated a semi-analytical approach for sensitivity matrix calculation in ERT using the MGLQ method. The proposed technique demonstrates a substantial advancement in computational efficiency, achieving a 15- 16-fold reduction in processing time compared to the AGKQ method, without compromising numerical accuracy. This performance gain is attributed to the method's fixed quadrature scheme and its effective analytical handling of singularities near electrodes which are critical bottlenecks in conventional approaches. The algorithm's robustness was verified by its excellent agreement with benchmark results and by satisfying the reciprocity principle, with a relative computational error of less than one percent. Furthermore, the analysis of sensitivity patterns for standard electrode arrays provided valuable geophysical insights that align with theoretical expectations, underscoring the method's practical utility for survey design and inversion reliability assessment. By offering a faster and reliable alternative for a core component of the ERT inversion process, this work facilitates more feasible and cost-effective large-scale geophysical imaging, with potential for future extension to more complex 3D and heterogeneous scenarios.

Appendices

Appendix A. Integral Singularity

In the integral calculation, there can be a singularity at the point where $x(j) = \frac{x_M + x_A}{2}$, where x_M and x_A represent the positions of two electrodes (M and A). To handle this singularity, the integral is divided into three parts based on the value of $x(j)$:

- When $\boldsymbol{x(j) < \frac{x_M + x_A}{2}}$,
- When $\boldsymbol{x(j) = \frac{x_M + x_A}{2}}$ (the singular point),
- When $\boldsymbol{x(j) > \frac{x_M + x_A}{2}}$.

For the singularity at $x(j_{singular}) = \frac{x_M + x_A}{2}$, the solution to the integral is given by the equation (Loke and Barker, 1995):

$$S_{ij}|j = jsingular = \frac{1}{2\pi^2}\left(\frac{\pi}{4a^3} - \frac{3a^2\pi}{32a^5}\right) \quad \text{(A1)}$$

where a^2 is calculated as:

$$a^2 = (0.5 - x_A)^2 + z_i{}^2 \ or \ a^2 = (0.5 - x_M)^2 + z_i{}^2 \quad \text{(A2)}$$

In these formulas, z_i is the vertical coordinate, and x_A and x_M are the positions of the current (A) and potential (M) electrodes, respectively.

To compute the Jacobian matrix at the singular point, we use the following formula:

$$\frac{\partial \phi_i(x,z)}{\partial m_j}|j = jsingular = \int_{z_i}^{z_{i+1}} S_{ij}.dz \quad \text{(A3)}$$

This equation is used to compute the sensitivity matrix in regions near singularities, typically around the electrodes, where accurate calculations are crucial. By incorporating this analytical approach into the algorithm, the method efficiently handles singularities without adding computational complexity. This ensures high accuracy even in areas with concentrated electrical fields, eliminating the need for costly numerical techniques to manage singular behavior.

Appendix B. four-electrode conditions

Equations A.1 and A.3 represent Jacobian matrix elements for a two-electrode array, such as a pole-pole configuration. According to Equation B.1, calculating the sensitivity for a four-electrode array requires four potential distributions.

$$\Delta\boldsymbol{\phi} = \Delta\boldsymbol{\phi_1} - \Delta\boldsymbol{\phi_2} - \Delta\boldsymbol{\phi_3} + \Delta\boldsymbol{\phi_4} \quad \text{(B1)}$$

As previously mentioned, each sensitivity calculation in a pole-pole array involves three states. When using four electrodes, the solution is derived from the superposition of four pole-pole calculations, each with its own three states. Consequently, a total of 12 states must be considered. In Figure B.1, 12 regions of the problem are presented. For instance, of region 1, $x_i < \frac{a+b}{2}$, $x_i = \frac{a+b}{2}$, $x_i > \frac{a+b}{2}$.

Here, $\Delta\varphi_1$ is applied between electrodes a and b, $\Delta\varphi_2$ between b and d, $\Delta\varphi_3$ between a and c, and $\Delta\varphi_4$ between c and d. When computing $\Delta\varphi$, some regions overlap (Regions 1, 2, and 8), resulting in nine independent regions. However, this overlap does not reduce the number of required conditions, all 12 conditions must still be evaluated for each x_i. Table B.1 lists these 12 conditions which must be verified before combining (summing) the individual calculations.

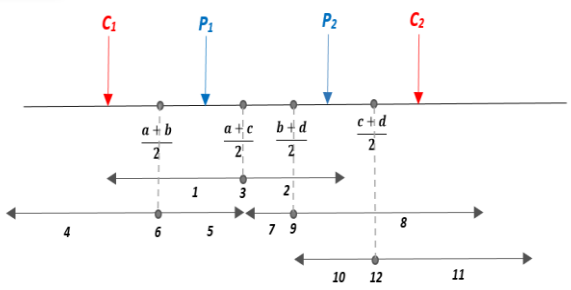

Figure B.1. Current electrodes and potential electrodes are shown with the red and blue arrows, respectively. Singularity points are also shown with green dots and 12 regions are determined.

Table B.1. 12 conditions of x(j). the different boundary conditions that have checked in the solution.

1.	1: $If\ x(j) < \frac{a+c}{2}$	2.	4: $If\ x(j) < \frac{a+b}{2}$	3.	7: $If\ x(j) < \frac{b+d}{2}$	4.	10: $If\ x(j) < \frac{c+d}{2}$
5.	2: $If\ x(j) > \frac{a+c}{2}$	6.	5: $If\ x(j) > \frac{a+b}{2}$	7.	8: $If\ x(j) > \frac{b+d}{2}$	8.	11: $If\ x(j) > \frac{c+d}{2}$
9.	3: $If\ x(j) = \frac{a+c}{2}$	10.	6: $If\ x(j) = \frac{a+b}{2}$	11.	9: $If\ x(j) = \frac{b+d}{2}$	12.	12: $If\ x(j) = \frac{c+d}{2}$

References

[1]. Loke, M. H. and Barker R. D., 1995, Least-squares deconvolution of apparent resistivity pseudosections. Geophysics 60, 1682-1690.

[2]. Spitzer, K., 1998, The three-dimensional dc sensitivity for surface and subsurface sources. Geophys. J. Int. 134, 736–746.

[3]. Barker, R. D., 1979, Signal contribution sections and their use in resistivity studies, Geophys. J. R. astr. Soc., 59, 123-129.

[4]. Boerner, D. E. and West, G. F., 1989, Fréchet derivatives and single scattering theory, Geophys. J. lnt., 98, 385-390.

[5]. McGillivray, P. R. and Oldenburg, D. W., 1990, Methods for calculating Frerchet derivatives and sensitivities for the non-linear inverse problem: a comparative study, Geophys. Prospect., 38, 499–524.

[6]. Park, S. K. and Van, G. P., 1991, Inversion of pole-pole data for 3-D resistivity structure beneath arrays of electrodes, Geophysics, 56, 951-960.

[7]. Sasaki, Y., 1994, 3-D resistivity inversion using the finite element method. Geophysics 55, 1839–1848.

[8]. Weller, A., Seichter, M. and Kampke, A., 1996. Induced-polarization modelling using complex electrical conductivities. Geophys. J. Int., 127, 387-398.

[9]. Loke, M. H, 2010, Tutorial: 2-D and 3-D electrical imaging surveys.

[10]. López-Sánchez, L., Mansilla-Plaza, M., Sánchez-de-laOrden, M., 2017, Geometric factor and influence of sensors in the establishment of a resistivity–moisture relation in soil samples. Journal of Applied Geophysics, 145, 1–11.

[11]. Danielsen, B. and Dahlin, T., 2010, Numerical modelling of resolution and sensitivity of ERT horizontal boreholes. Journal of Applied Geophysics 70, 245–254.

[12]. Leontarakis K. and Apostolopoulos G. 2012. Laboratory study of the cross-hole resistivity tomography: the model stacking (MOST) Technique. Journal of Applied Geophysics 80, 67–82.

[13]. Tso, C.-H. M., Kuras, O., Wilkinson, P., Uhlemann, S., Chambers, J., Meldrum, P., Graham, J., Sherlock, E. and Binley, A., 2017, Improved characterisation and modelling of measurement errors in electrical resistivity tomography (ERT) surveys. Journal of Applied Geophysics. Advance online publication.

[14]. Ghanati, R., and M. Fallahsafari, 2022, Fréchet derivatives calculation for electrical resistivity imaging using forward matrix method: Iranian Journal of Geophysics, 15, 153–163

[15]. Azadi and Ghanati, 2025, Optimization-driven two-dimensional Gauss–Legendre quadrature for fast Jacobian assembly in geophysical exploration, the 7th Applied Geophysics Conference in Oil Exploration, Tehran.

[16]. Burden, R. L., Faires, J. D., Reynolds, A. C., 1981, Numerical Analysis. Prindle, Weeber & Schmidt, Massachusetts.

[17]. Günther, T., 2004, Inversion Methods and Resolution Analysis for the 2D/3D Reconstruction of Resistivity Structures from DC Measurements, PhD thesis. University of Mining and Technology, Freiberg.

[18]. Geselowitz, D. B., 1971, An Application of Electrocardiographic Lead Theory to Impedance Plethysmography, in IEEE Transactions on Biomedical Engineering, 18, 38-41.

[19]. Press, W. H., Teukolsky, S.A., Vetterling, W.T. & Flannery, B.P., 1986. Numerical Recipes, Cambridge University Press.

[20]. Churchhouse, R. F. (ed.), 1981, Handbook of applicable mathematics. Vol. III: Numerical methods: John Wiley & Sons, Inc.

[21]. Barker, R. D., 1992, A simple algorithm for electrical imaging of the subsurface: First Break, 10, no. 2, 53-62.

[22]. Binley, A. and Kemna, A., 2005, DC resistivity and induced polarization methods. In Y. Rubin & S. S. Hubbard (Eds.), Hydrogeophysics (pp.129–156). Dordrecht, Netherlands: Springer.